Traveling density wave models for earthquakes and driven threshold systems

John B. Rundle
Departments of Geological Sciences and Physics and Cooperative Institute for Research in Environmental Sciences, University of Colorado, Boulder, Colorado 80309

W. Klein
Center for Computational Science and Department of Physics, Boston University, Boston, Massachusetts 02215

Susanna Gross
Cooperative Institute for Research in Environmental Sciences, University of Colorado, Boulder, Colorado 80309

C. D. Ferguson
Center for Computational Science and Department of Physics, Boston University, Boston, Massachusetts 02215
(Received 10 January 1997)

Driven threshold systems are now used to model sandpiles, earthquakes, magnetic depinning transitions, integrate-and-fire neural networks, and driven foams. We analyze a physically motivated model which has many of the same properties as the hard threshold models, but in which all of the nonequilibrium physics is obtained from a Lyapunov functional. The ideas apply to mean-field systems, and lead to a number of predictions, including scaling exponents and metastable lifetimes for nucleating droplets. The former predictions are supported, for example, by data observed for earthquake fault systems. An interesting consequence of the model is that time appears as a scaling field, leading to temporal scaling laws similar to those observed in nature. [S1063-651X(97)09307-0]

PACS number(s): 05.40.+j

I. INTRODUCTION

A variety of nonlinear, driven systems have dynamics that have been modeled with thresholds. Common to these models is a repetitive process in which the force or potential at a lattice site is persistently increased by the externally supplied force, until a sharp threshold is reached when a sudden jump to a new state occurs. During the jump, the force is greatly reduced, after which the process begins again. Depending on the degree to which each site is coupled to its neighbors, other sites will be induced to jump at the same time. Probably the two most widely known examples are the sandpile model [1] of self-organized criticality, and the Burridge-Knopoff (BK) slider block model [2] for earthquakes. In the former, a lattice accumulates particles, or is tilted, until a critical slope (threshold) is reached at which avalanches (clusters of failed sites) begin to occur. In the simplest versions of these models, avalanches of all sizes occur, leading to a family of critical exponents, the mean-field values of which [3] have been shown to be identical to those for mean-field percolation (the same as spinodal exponents). Similarly, in the slider block models [2,4], a loader plate increases the stress on a network of coupled sliding blocks until the static friction threshold is reached. At that point, one or more of the blocks begin to slide, still subject to a dynamical friction stress. Avalanches (clusters) of failing blocks of all sizes occur, again leading to another family of critical exponents.

The basic picture of a persistently driven dynamical system displaying threshold dynamics is evidently a common model for a variety of physical systems [2,5–7], including magnetic depinning transitions [6] and slowly driven foams [7]. Yet a basic question remains as to whether these systems are best described as residing near a critical point in the state space of the system, or as systems that occasionally display nucleation events. The latter are avalanches involving the entire system that occur significantly more frequently than would be expected on the basis of the observed frequency of small events. Data from laboratory [8] and field observations [9,10] apparently indicates that both real sandpiles and earthquake faults often display phenomena associated with nucleation events, in which the entire sandpile or fault fails following a series of smaller events.

In this work, we present the ''traveling density wave'' (TDW) model [11] that may be useful for understanding the physical processes of driven nonlinear threshold systems. The TDW Lyapunov functional is similar to the density wave Hamiltonian [12,13] used to describe charge and spin density waves. In this model, the system is persistently driven to failure by means of external forces, and the sudden jump of a site to a new state is a nucleation event. Moreover, since the nucleation occurs near the mean-field spinodal, which behaves as a line of critical points, a scaling regime is observed that has the ''magnetic'' spinodal scaling exponents. The scaling fields for the TDW model are (1) time and (2) a parameter Λ involving the wavelength and amplitude of the cohesive forces across the sliding surface, and the elastic constants of the surrounding elastic medium. For example, nucleation events (''earthquakes'') as well as ordinary critical phenomena (''fault creep'') are predicted, and have been seen in the simulations discussed below. ''Aftershock'' and ''foreshock'' events are predicted, as well as an Omori law [9] for both aftershocks and foreshocks that has a temporal scaling exponent $p=1$, the value most often observed in nature, $p_{\rm obs}\approx 1$.

To motivate the foundations of the traveling density wave model, which may have general applications to a wide variety of other systems, we return to the prototypical threshold system of an earthquake fault driven by tectonic plate motion. We discuss the manner in which the TDW model arises in this context, followed by an investigation of its properties.

II. MODELS FOR EARTHQUAKES AND FRICTIONAL SLIDING

A central problem in understanding earthquakes lies in clarifying the physics of the frictional sliding processes [14]. Current modeling approaches [2,4,15–19] rely on friction laws that are of either the cellular automaton (CA) jump-rule type; the simple BK model with inverse velocity dependence; or the experimentally determined, Dieterich-Ruina (DR) parametrized state-variable model. While the latter is based on the idea that two surfaces under shearing stress are never actually stationary, recent experimental data [20,21] raise new questions about the validity and applicability of this critical assumption. It seems clear from this new data, that real fault surfaces, which are not clean, smooth and dust free, will not be described by the simplistic rate and state-variable description. These data indicate that the experimental surfaces do experience arrest, and in that case the DR friction laws predict an infinite and unphysical value of static friction. Moreover, the DR friction laws are not applicable [20,21] throughout the entire sliding regime, the data upon which they are based having been obtained only at low sliding velocities and over small total slip distances. In fact, as sliding progresses, velocity weakening behavior becomes transformed into velocity strengthening behavior as the surfaces accumulate dust and gouge between them. Velocity strengthening behavior is incompatible with frictional instabilities. On the other hand, the Burridge-Knopoff-Carlson-Langer friction law was simply assumed, as described in Ref. [2], and its observational motivation is not clear. Moreover, it is not clear what value of mass to use in the BK models, inasmuch as it is not clear what the massive elements are intended to represent. Finally, the CA friction laws represent the effects of static and dynamic friction by specifying a rupture threshold, and a residual stress at which motion ceases. While the CA friction models only approximate macroscopic friction (see Sec. IX), they are better representations of the processes operating on random disordered surfaces. Problems such as these, with all of these friction models, have prevented the formulation of a unifying and physically self-consistent viewpoint of the process of frictional sliding.

An important recent development [15,22] has shown that classes of mean-field CA models can be described by a spatially and temporally coarse grained field theoretic formulation, and that these models can often be treated as equilibrium models. The details of the field theory will be presented elsewhere [23]. The fact that mean-field models can be treated in a manner similar to equilibrium systems is based on an extensive series of simulations of mean-field and ''mean-field-like'' CA models, which we now describe.

III. CELLULAR AUTOMATON SLIDER BLOCK MODELS

Nearest neighbor CA models are often called slider block models (Fig. 1). The first such model was the BK model. It was also the first model to capture the scaling phenomena observed during earthquakes. The basic idea is that slider block models represent the kind of microscopic physics that would be found at the smallest scales on a frictional sliding surface. The CA slider block models are distinguished from the original massive BK slider block model [2] in that the position of each block through time is obtained from an update rule, instead of by solving a set of N coupled differential equations for N-element models, as is the case in the BK model. Farther neighbor models can also be implemented to represent elastic continua [11,14,24] using long range coupling springs whose spring constants decay with distance r as $1/r^3$. An advantage of massless CA models is that the dynamics of large N models can be examined on even modest workstations, which can be important when correlation lengths are large and finite size effects are important.

Cellular automaton models are ''freshman physics'' models for friction that have been widely studied in the literature [4,5,14,25–29]. Consider a two-dimensional array of N frictional blocks (or lattice site) with each block connected to its nearest neighbor by coupling springs with spring constant K_C, and to a loader plate by a loader spring with spring constant K_L. The loader plate translates at velocity V, increasing the force on each sticking block until it slips when the force (stress) exceeds the static friction. In these models, a static failure threshold σ^F is prescribed, along with a residual stress σ^R. When the stress on a site increases, either gradually or suddenly, to equal or exceed σ^F, a sudden jump in slip occurs that takes the stress at the site down to a residual value σ^R. The exact details of the jump process, and whether it occurs synchronously or asynchronously with the jumps at other sites, is a model-dependent decision. These models assume a separation of time scales, the time scale for long term motion being far larger than the time scale on which adjustment of the slip state occurs. While the advantage of this friction model is ease of computational implementation, the disadvantage is that it captures the physics of stick-slip sliding best for disordered microscopic surfaces, and allows considerable latitude in specification of the jump mechanism.

More generally, these lattice threshold CA models are nonequilibrium systems that fluctuate around a time-averaged steady state. In a sense, these systems are similar to equilibrium systems that also fluctuate around the time-average equilibrium state. A subset of these models are deterministic, and are known to have periodic limit cycles [22,26]. Another class of models [30–32], also deterministic, do not have a limit cycle attractor, but instead fluctuate in a complicated manner about a constant energy. The major focus here is a third and separate class of slider block models that have a stochastic dynamics, and in which the blocks are massless, and the jumps are random variables uniformly distributed about an average value.

IV. STOCHASTIC MODELS, MEAN-FIELD, AND BOLTZMANN STATISTICS

As motivation, consider a typical equilibrium system for which the total energy $E_T \approx$ constant, except for small fluctuations, the mean square probability of which decrease in magnitude as $1/\sqrt{N}$, where N is the number of particles (or

degrees of freedom or modes). In such a model, the internal energy E_i of each independent field variable (molecules, spins, etc.) executes small fluctuations about the time-averaged mean energy. Assuming that the system obeys the postulate of equal *a priori* probability, the method of most probable distributions [32] can then be used to show that the expected distribution of block energies is Boltzmann. Dividing the possible energy states into $\{q=1,\ldots,Q\}$ energy banded $E(q)$ occupied with probability $P(q)$, detailed balance requires that

$$\sum_q P(E_q)=1,$$

$$\sum_q P(E_q)E_q=E_T\approx\text{const.} \tag{1}$$

From Eq. (1) and the assumption of equal *a priori* probability it is simple to show that the probability of a state $P(E_q)\propto \exp[-E_q/T_{\rm SB}]$, the Boltzmann distribution, where $S_{\rm SB}$ is the lattice average energy per degree of freedom [32] ($T_{\rm SB}$ is the mean energy, the ''temperature'').

We apply these ideas to the slider block model. Consider the Hamiltonian [15] for models with arbitrary range interactions having coupling springs of fixed strength K_C

$$H_{\rm SB}=\frac{1}{2}\sum_i \left\{K_L[\phi_i-V\tau]^2+\frac{1}{2}K_C\sum_{j=\rm int}[\phi_j-\phi_i]^2\right\}. \tag{2}$$

The sum over i is over all sites in the lattice, and the sum over j is over all interacting blocks within the range of interaction R but excluding site i. The time τ represents a loading time scale; it must be present inasmuch as loading due to the far field velocity V must occur prior to failure. The order parameter field is the slip deficit $\phi_i(t)=s_i(t)-Vt$, $s_i(t)$ is the slip of block i at time t. The value of $H_{\rm SB}$ for a particular configuration $[\phi_i]$ is $E_{\rm SB}=H_{\rm SB}(\phi)$. The force (stress) σ_i on block i is

$$\sigma_{{\rm SB},i}=-\partial H_{\rm SB}/\partial\phi_i=-\left\{K_L[\phi_i-V\tau]+K_C\sum_{j=\rm int}[\phi_j-\phi_i]\right\}. \tag{3}$$

Expression (2) can be formally obtained [15] from the expression for the elastic strain energy of a fault embedded within an elastic continuum, in the presence of short range and long range cutoffs, by the use of a gradient expansion. For the nearest neighbor models, the spring constants K_L and K_C are then related respectively to the 0th and 2nd moments of the stress Green's function. For the moment, we specialize to models with $V\gtrsim 0$, in which only one avalanche occurs following each loader plate update. Slider block models with nonzero V are discussed further in Ref. [14].

A rule to generate the dynamics must be specified. The simplest example is the modified Mohr-Coulomb friction law, in which each block has a prescribed static failure threshold σ_i^F and a residual stress at which the block sticks σ_i^R. The dynamics are generated by a jump rule giving the position of the block as a function of the state of stress on the block. Jump rules such as these can be either deterministic or stochastic. The basic jump rule is

$$s_i(t+1)=s_i(t)+J(\sigma_i)\Theta(\sigma_i-\sigma_i^F), \tag{4}$$

where $\Theta(x)$ is a Heaviside step and the failure threshold σ_i^F is spatially dependent. Examples [33] of deterministic jump functions $J(\sigma_i)=\Delta s_i$ include

$$J_1=(\sigma_i-\sigma_i^R)/K_T,$$
$$J_2=(\sigma_i^F-\sigma_i^R)/K_T, \tag{5}$$

where σ_i^R is a residual stress and K_T is the total spring constant ($K_T=K_L+2dK_C$, d is the dimension of space). This expression is valid also for a model with longer range springs (interactions), in which each block interacts with N_R other blocks via springs with spring constants K_C. Each block jumps from its current stress at failure to the position having the specified residual stress σ_i^R, thus Eqs. (4) and (5) are examples of a deterministic rule.

A stochastic jump rule can also be used [15]. For these models, the jump is given by

$$J_s=J_1(1-W\rho), \tag{6}$$

where W is a (constant) width chosen from $0\leqslant W\leqslant 1$, and ρ is a uniformly distributed random number on $\rho\in[0,1]$.

In the models described in the following, it will be assumed that $\sigma_i^F=\sigma^F$ are constant, and $\sigma_i^R=\sigma^R$ are constant. Noise in these models arises both from the initial conditions and from randomness in the jump described by W, which represents random microscopic processes associated with wear and spatially inhomogeneous properties of the sliding surface. Thus, in the limit of $V=0$, the parameters that should completely determine model behavior are K_L, K_C, σ^F, σ^R, and W.

To understand the results of the simulations carried out below, we observe that the slip deficit $\phi_i(t)$ of a block fluctuates around a time-averaged value $\overline{\phi_i}$

$$\overline{\phi_i}\equiv\frac{1}{T}\int_0^T\phi_i(t)dt. \tag{7}$$

The fluctuating part $\zeta_i(t)$ is then defined by

$$\phi_i(t)=\overline{\phi_i}+\zeta_i(t). \tag{8}$$

For convenience in analyzing data obtained in simulations using the jump (6), we normalize the fluctuation $\zeta_i(t)$ to unity by defining the variance ω [2]:

$$\omega_1^2\equiv\frac{1}{T}\int_0^T[\zeta_i(t)]^2dt. \tag{9}$$

Then

$$\zeta_i'(t)\equiv\frac{1}{\omega_i}\zeta_i(t). \tag{10}$$

Considering models with $V\to 0$, the Hamiltonian (2) can now be written as

$$H_{\rm SB}\equiv H_0+H_1+H', \tag{11}$$

where the various terms are defined as

$$H_0 \equiv \frac{1}{2}\sum_i \left\{ K_L(\overline{\phi_i})^2 + \frac{1}{2}K_C \sum_{j=\text{int}} [\overline{\phi_j} - \overline{\phi_i}]^2 \right\},$$

$$H_1 \equiv \sum_i \omega_i \left\{ K_L \overline{\phi_i}\zeta_i' + \frac{1}{2}K_C \sum_{j=\text{int}} [\gamma_{ij}\zeta_j' - \zeta_i'][\overline{\phi_j} - \overline{\phi_i}] \right\}, \tag{12}$$

$$H' \equiv \frac{1}{2}\sum_i \omega_i^2 \left\{ K_L(\zeta_i')^2 + \frac{1}{2}K_C \sum_{j=\text{int}} [\gamma_{ij}\zeta_j' - \zeta_i']^2 \right\},$$

and where

$$\gamma_{ij} = \frac{\omega_j}{\omega_i}. \tag{13}$$

We accumulated time-averaged statistics of the energy distribution corresponding to the energy given by Eqs. (11) and (12). Taking the time average $\overline{H_{\text{SB}}}$ of H_{SB} in Eq. (11), it can be observed that

$$\overline{H_0} = H_0,$$

$$\overline{H_1} = 0, \tag{14}$$

$$\overline{H'} \neq 0.$$

H_0 is a constant, H_1 executes small fluctuations about 0, and H' fluctuates about some nonzero value. The fluctuations in H_1 will be expected to have a Gaussian distribution since H_1 is clearly a linear sum of random variables ζ_i'.

Since we are interested in the nonzero time-averaged occupating numbers n_q for the various energy bands centered on E_q, we focus attention on the last of Eqs. (12). We therefore define (see below)

$$\overline{H'} \equiv 2T_{\text{SB}} \equiv \sum_q n_q E_q. \tag{15}$$

By comparison of Eq. (15) with Eqs. (1) and (2), we surmise that the number n_q of blocks that occupy energy levels E_q should display Boltzmann statistics, assuming that all configurations have equal *a priori* probability.

We expect that the property of microscopic chaos [32] will exist in the slider block models when the interaction between neighboring blocks is large enough to self-organize the blocks against the competing stochastic noise from the block jumps. In turn, some level of stochastic noise must be present, particularly for small values of K_C, to prevent the blocks from phase locking into a limit cycle [28]. In other words, the random jump function introduces a stochastic noise, allowing the system to explore its phase space effectively. Since $R = (K_C/K_L)^{1/2}$ is a measure of the range of interaction, models with large values of R are expected to display mean-field characteristics. Mean-field models with a noise level are more likely to demonstrate Boltzmann statistics, and to have decreasing amplitude fluctuations at all but the largest wavelengths. Therefore, the assumption $\Sigma_q n_q E_q \approx$ const is more likely to be valid.

For mean-field slider block models in two dimensions [15], the distribution of energies is not $p(E_q) \propto \exp[-E_q/T_{\text{SB}}]$, but $p(E_q) \propto E_q \exp[-E_q/T_{\text{SB}}]$. It is clear that the energy E of a block is the sum of energies contained within all the springs connected to that block [see Eq. (2)]. The energy in the ith spring is itself proportional to the square of a stochastic variable $\phi_i(t)$, which is maintained in a random state as a result of the random jump amplitude W. Thus E is proportional to the sum of the squares of a set of random variables. Standard results from probability theory [34] indicate that with suitable normalization of the random variables, we should expect E to be distributed with a χ square distribution with ν degrees of freedom, i.e., $p(E) \propto E^{\nu/2-1} \exp[-E/T_{\text{SB}}]$.

For large values of K_C/K_L, one would expect that the coupling springs would store most of the energy. For the nearest neighbor models studied here, this implies that $\nu = 4$, and $p(E) \propto E \exp[-E/T_{\text{SB}}]$. However, this reasoning seems inconsistent with the results obtained by the method of most probable distributions [32], because the number of degrees of freedom for a gas of particles is effectively infinite. One would not, therefore, expect to obtain the simple result $p(E) \propto \exp[-E/T_{\text{SB}}]$.

A different, and perhaps more consistent, line of reasoning is based on the fact that the fractal dimension D_f for mean-field systems [35] is $D_f = 4$. If the number of degrees of freedom ν for each block (the effective dimension) is then assumed to be $\nu = D_f$, one obtains the observed result. Moreover, for the simple case derived using the two constraints of Eq. (1), ν is $D_f = 4$ minus the two constraints of Eq. (1). Hence $\nu = D_f - 2 = 2$ degrees of freedom, and $p(E) \propto \exp[-E/T_{\text{SB}}]$ as found from the method of most probable distributions. Although preliminary results [22,23] seem to validate this approach, we are now in the process of more extensive testing using simulations of models with long range springs.

To determine whether these predictions of Boltzmann statistics are valid, the energies of blocks in a nearest neighbor slider block simulation having random jumps were measured [15]. For an unbounded system, a normalized energy functional $H''(\zeta_i)$ can be written in terms of the normalized slip deficit ζ_i' on the ith block as

$$H'' = \frac{1}{2}\sum_i \left\{ K_L \zeta_i'^2 + \frac{1}{2}K_C \sum_{j=\text{int}} [\zeta_j' - \zeta_i']^2 \right\}. \tag{16}$$

Measuring the energies was accomplished by defining 10 000 energy bands centered on each E_q, $[q = 1, \ldots, 10\,000]$. Upon termination of all block instabilities following a loader plate update, the number of block energies falling into each narrow energy band are counted. Defining

$$P(E_q) = n_q/N \tag{17}$$

as the probability density function, and assuming that the $P(E_q)$ are normalized Boltzmann functions as described above

$$P(E_q) = \frac{E_q}{T_{\text{SB}}^2} \exp[-E_q/T_{\text{SB}}], \tag{18}$$

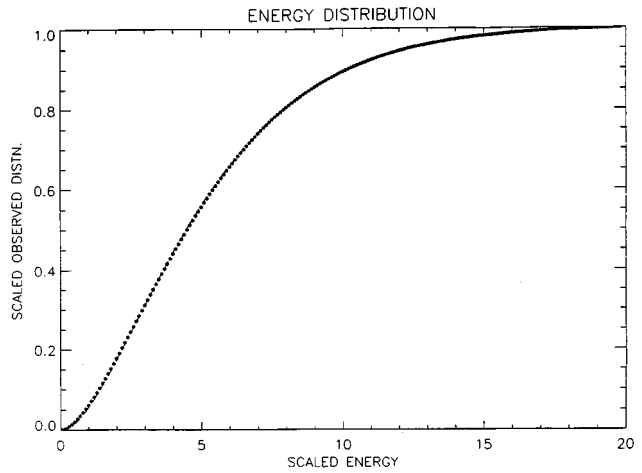

FIG. 1. Cumulative distribution function of block energies E_q from our simulation (dots) using Eqs. (19) and (20). Model parameters for the plot are $K_L=1$, $K_C=25$, $\sigma^F=35$, $\sigma^R=-0.35$, and $W=0.1$. The mean scaled energy is 5.34, or equivalently $T_{\rm SB}=2.67$. The dashed line between the dots is Eq. (19) using $T_{\rm SB}=2.67$ as the decay length. This is a mean-field model, and illustrates the quality of fit between simulation data and theory.

the expected normalized cumulative distribution function (CDF) $F(E')$ is obtained from

$$F(E')=\int_0^{E'} E'\,\exp\,[-E']dE'$$

$$=1-(1+E')\exp[-E'],\quad E'=E/T_{\rm SB}. \quad (19)$$

The quantity $T_{\rm SB}$ can be related to the measured time and lattice average of the energy $H'(t)$, which we denote as $\langle\overline{H'}\rangle$. Using Eq. (18), we obtain the time-average energy per block $T_{\rm SB}$ as

$$T_{\rm SB}=(1/2)\langle\overline{H'}\rangle. \quad (20)$$

Equations (18)–(20) represent a prediction, with no free parameters, of the energy distribution obtained from simulation data.

It was emphasized in Ref. [11] that Boltzmann statistics apply only to mean-field models. An example of a mean-field Boltzmann model is given in Fig. 1, which visually shows the quality of the fit between the numerically measured energies for the normalized energy functional H'' and the predicted curve. The CDF prediction has a decay length that is obtained by measuring $(1/2)\langle\overline{H''}\rangle$. That value is then used together with Eq. (19) in evaluating the CDF, the dashed curve. The dashed, theoretical CDF curve is almost indistinguishable from the experimentally determined CDF measured from the simulations (dots).

Figure 2 shows a comparison between two mean-field models with different model parameters, thus different temperatures $T_{\rm SB1}$ and $T_{\rm SB2}$. In that figure, the logarithm of the ratio P_1/P_2 is plotted against energy E, where the P's are the Boltzmann functions in Eq. (18). Thus on a semilog plot, $\ln(P_1/P_2)$ should be a linear function of E, with slope determined by $1/T_{\rm SB1}-1/T_{\rm SB2}$. Figure 2 confirms this result.

Figure 3 illustrates the relationship between the temperature $T_{\rm SB}$ and the model parameters K_L, K_C, σ^F, and σ^R. Since the energy is stored in the springs, the energy should be related to a quantity such as $\sim$ (spring constant) $\times$ (measure of jump size) [2]. Thus we search for a relation such as

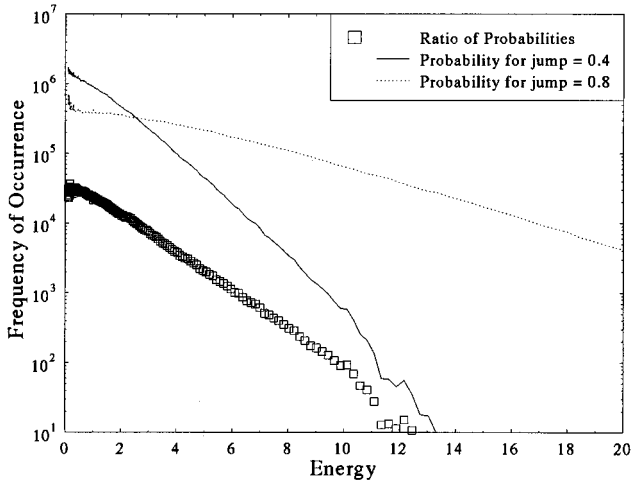

FIG. 2. Probability density functions for two mean-field models $[P_1(E),P_2(E)]$, together with $\ln\{P_1/P_2\}$, plotted against E. Both P_1 and P_2 are expected to have the form of Eq. (18), but their ratio should cancel the density of states prefactor, leaving a pure Boltzmann factor, $\exp[-E(1/T_1-1/T_2)]$. On a semilog plot, this function plots as a line, given by the squares.

$$T_{\rm SB}\propto Ex[K_T J^2], \quad (21)$$

where $Ex[\ ]$ is the expectation operator arising from the stochastic nature of the random variable ρ [see Eq. (6)]. Using Eq. (6), the expectation $Ex[K_T J^2]$ is easily shown to be

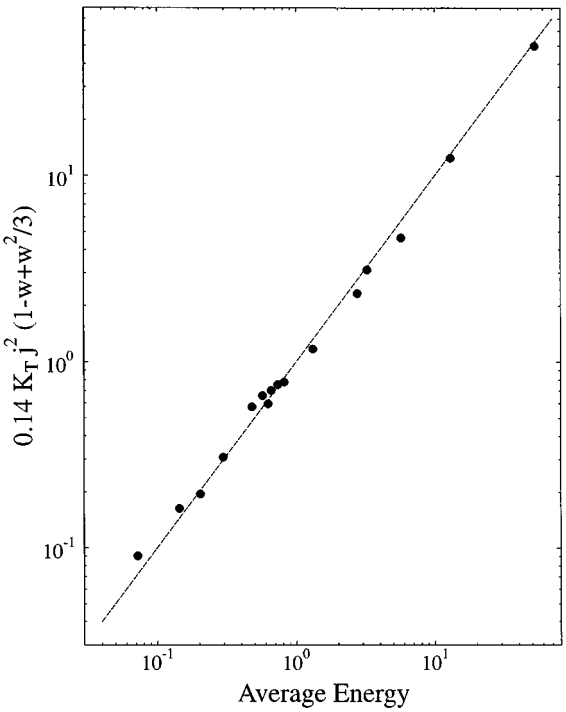

FIG. 3. Average energy $2T_{\rm SB}=\langle\overline{H'}\rangle$ of models against the quantity given on the right side of Eq. (24). Dashed line has a slope of 1.

$$Ex[K_T J^2] = Ex[K_T J_0^2 (1 - W\rho)^2] = K_T J_0^2 [1 - W + \tfrac{1}{3} W^2] \tag{22}$$

with

$$J_0 = \frac{\sigma^F - \sigma^R}{K_T}. \tag{23}$$

In Fig. 3, we plot the average energy $2T_{\rm SB} = \langle \overline{H'} \rangle$, against the right hand side of Eq. (22) multiplied by the constant number 0.14. The latter is obtained by requiring that the best fitting line have a slope of 1, and that the best fit line pass through the origin. The ''temperature'' or energy of slider block models is thus given by

$$T_{\rm SB} \approx 0.07 [K_T J_0^2 (1 - W + \tfrac{1}{3} W^2)] \tag{24}$$

to within small error. The factor of 0.07 represents the ''Boltzmann constant'' for this class of models, and is evidently model-class dependent. The mean-field region is the low energy region at the lower left corner of the figure. It can be seen that Eq. (24) provides a good representation of the average energy of the model, even for non-mean-field models (upper right portion of the figure).

The results obtained here depend only on two conditions: (1) the system executes small fluctuations around a state of fixed internal energy; and (2) that enough noise is present to allow the system to fully explore its phase space. It can also be shown that a separate condition requires that the rate of forcing be low [22]. Because this line of reasoning does not depend on the massless nature of the slider blocks, we expect that similar results will be observed in some classes of massive slider block simulations as well. Since the noise amplitude required to generate the Boltzmann distribution decreases as the mean-field regime is approached, we also predict that the amplitude of the external noise needed to produce the Boltzmann distribution should be vanishingly small in the mean-field limit. It is therefore likely that Boltzmann fluctuations will be important in nature, and that these fluctuations may be the origin of extended spatial correlations observed in real earthquake fault systems (see, for example, Ref. [36]).

V. TRAVELING DENSITY WAVE MODEL

To our knowledge, all models for earthquakes and frictional sliding that have been examined to date begin by postulating a dynamical equation to describe the evolution of the system. However, to begin with an assumption of a Newtonian balance of forces for such a dissipative system leaves us with questions, such as (1) how to understand the energetics of the jump transitions and (2) the physical origin of scaling in these models, as well as the origin and identity of the scaling fields. An intuitively more appealing approach would base the physics on the construction of a functional potential, with the resulting force balance equations arising as an Itô-Langevin equation obtained from variation of the functional potential. This idea is the basis of the traveling density wave model.

Support for this approach arises from the result described above that mean-field CA models for friction have a Boltzmann energy distribution. Using this as the starting point, Ref. [22] has shown how to construct a spatially and temporally coarse grained Itô-Langevin equation for a mean-field CA model. The existence of such an Itô-Langevin equation in turn implies the existence of a functional potential for the dynamics. We are therefore motivated to develop a formalism, based both upon theoretical ideas as well as upon laboratory and field data [37–42], to describe the threshold dynamics of these driven nonlinear systems. We will again couch the discussion in terms of a model for earthquakes, although the final result clearly has a more widespread applicability.

We begin by considering two elastic media in contact at a surface upon which slip $s(\mathbf{x},t)$ can occur in response to applied shear stress. Sliding is driven [43] by the imposition of a spatially constant displacement s_B or stresses σ_B applied at distances remote from the slip surface. For such a system, the elastic stress $\sigma^e(\mathbf{x},t)$ on the slip surface at $(\mathbf{x},t)$ can be written in terms of (1) a stress Green's function (spatial interaction), written schematically as $T(\mathbf{x}-\mathbf{x}')$; (2) the externally applied shear stress σ_B, and (3) the slip deficit $\phi = s(\mathbf{x},t) - s_B$

$$\sigma^e(\mathbf{x},t) = \int T(\mathbf{x}-\mathbf{x}')\,\phi(\mathbf{x}',t)\,d^2\mathbf{x}' + \sigma_B\,. \tag{25}$$

Note that the elastic stress is a functional of ϕ, which we denote as $\sigma^e[\phi]$, and that we consider one side of the surface ''fixed,'' with a coordinate system $\mathbf{x}$ attached to the ''moving'' side.

There is also a frictional stress σ^f on the surface resisting slip. In formulating the general characteristics of the friction, we refer to the extensive literature [37–42] on macroscopic friction and wear of solids, particularly the extensive compilation of data described in Refs. [37] and [38]. We note that σ^f arises from the cohesion between the sliding surfaces, and that the contact between irregular surfaces will vary as sliding progresses. Following Ref. [38], we therefore take σ^f at each location to be a functional

$$\sigma^f = \sigma^f(s(\mathbf{x},t); c; r). \tag{26}$$

In Eq. (26), $s(\mathbf{x},t)$ is the total slip experienced by the point at coordinate $\mathbf{x}$ at time t, c represents a set of parameters describing the cohesion between the surfaces, and r represents a set of random parameters. Both of the parameter sets represented by c and r are in general site (location) and time dependent. Time dependence describes irreversible wearing of the surface, i.e., random alteration of surface properties as a result of microscopic surface damage during sliding. Note that σ^f is a function of space and time through the space and time dependence of s, c, and r. Also, c should depend explicitly on the normal stress σ_N pushing the surfaces into contact.

Now we consider a state of deformation of the system (solid+surface) induced by a far field displacement s_B. The balance of forces [43,44] on the surface requires that

$$\sigma^e[\phi] = \sigma^f[\phi + s_B; c; r] \tag{27}$$

using the definition of ϕ. We are interested here in models with $\sigma_B = 0$, and in which the boundaries are translating uni-

formly, so that $s_B = Vt$, where V is the velocity of the ''moving'' side with respect to the ''fixed'' side. Equation (27) is then

$$\sigma^e[\phi] = \sigma^f[\phi + Vt]. \tag{28}$$

We remark that Eq. (28) has a very simple interpretation. The instantaneous balance of forces at a site $\mathbf{x}$ can be viewed in the (σ,ϕ) plane as the intersection of a fixed curve $\sigma^e[\phi]$ with a leftward moving (traveling) wave $\phi^f[\phi + Vt]$. This observation motivates the TDW name for the model.

The existence of a functional potential $U[\phi]$, which follows from prior results [22] is equivalent to the assumption that Eq. (28) is the Euler-Lagrange equation arising from that potential [43,44]. We therefore define the potential $U[\phi]$

$$U[\phi] = E[\phi] - S[\phi + s_B, \phi], \tag{29}$$

so that Eq. (28) arises from $U[\phi]$ by functional differentiation

$$\frac{\delta U}{\delta \phi} = 0. \tag{30}$$

U is a Lyapunov functional that plays a role similar to an equilibrium ''free energy functional.''

Construction of U proceeds by taking proper account of both the elastic and the cohesive forces acting across the sliding surface. It is straightforward [15,43,44] to show that the ''elastic energy'' $E[\phi]$ exists and has the form

$$E[\phi] = \int \int \{ -\tfrac{1}{2}[T(\mathbf{x}-\mathbf{x}')\phi(\mathbf{x},t)\phi(\mathbf{x}',t)d^2\mathbf{x}'] + \sigma_B \phi(\mathbf{x},t)\} d^2\mathbf{x}. \tag{31}$$

S is likewise related to σ^f by functional differentiation

$$\sigma^f = -\frac{\delta S}{\delta \phi}. \tag{32}$$

The functional $S[\phi + s_B, \phi]$ defines the energy associated with the cohesive forces acting on the surface [44]. Since the cohesive force σ^f is by assumption bounded and continuous on the interval $(-\infty,\infty)$, the Fourier expansion theorem [45] states that σ^f has a cosine series representation in the variable $(\phi + s_B)$. Using expansion parameters A_n, κ_n, and $h = A_0$, $S[\phi + s_B, \phi]$ can then be obtained by functional integration of σ^f

$$S[\phi + s_B, \phi] = \int \left[\sum_n A_n \cos\{\kappa_n(\phi(\mathbf{x},t) + s_B + \varepsilon_n)\} - h\phi(\mathbf{x},t) \right] d^2\mathbf{x}. \tag{33}$$

The parameters A_n, κ_n, ε_n, and h describe the cohesive (''c'') properties of the frictional forces. These parameters can also have a random part (''r'') associated with processes of ''wearing'' on the surface, i.e., general time dependent changes in cohesion associated with the accumulation of irreversible surface damage.

Now suppose that the system resides in a nonminimal potential energy state that does not satisfy Eq. (30). It is reasonable to assume that the fault system evolves persistently toward minimum potential energy, and thus greater stability

$$\delta U = \delta\phi \left(\frac{\delta U}{\delta \phi} \right) \leqslant 0. \tag{34}$$

Equation (34) then implies that to first order in $\delta\phi$, the evolution of the system in the presence of noise is obtained by solving the Itô-Langevin equation

$$\frac{\partial \phi}{\partial t} = -\Gamma \frac{\delta U}{\delta \phi} + \eta(\mathbf{x},t). \tag{35}$$

The noise is assumed to be δ correlated

$$\langle \eta(\mathbf{x},t)\,\eta(\mathbf{x}',t') \rangle = \beta^{-1}\delta(t-t')\,\delta(\mathbf{x}-\mathbf{x}'), \tag{36}$$

and β is a constant inverse noise amplitude.

To explore the consequences of these ideas, suppose that σ^f is dominated by only one of the Fourier terms for some wave number κ

$$U[\phi] = \int \int \{ -\tfrac{1}{2}[T(\mathbf{x}-\mathbf{x}')\phi(\mathbf{x},t)\phi(\mathbf{x}',t)d^2\mathbf{x}'] - 2\gamma_c \cos[\kappa\{\phi(\mathbf{x},t) + Vt + \varepsilon\}] + h\phi(\mathbf{x},t)\} d^2\mathbf{x}. \tag{37}$$

Both $2\gamma_c$ and h depend in general on the normal stress σ_N, which in turn depends [46] on V. Using Eq. (35), the corresponding Itô-Langevin equation is

$$\frac{\partial \phi(\mathbf{x},t)}{\partial t} = \Gamma \left\{ \int T(\mathbf{x}-\mathbf{x}')\phi(\mathbf{x}',t)d^2\mathbf{x}' - 2\gamma_c\kappa \sin\{\kappa\phi(\mathbf{x},t) + Vt + \varepsilon(\mathbf{x},t)\} - h \right\} + \eta(\mathbf{x},t). \tag{38}$$

The ''thermodynamics'' of this model are obtained by searching for spatially uniform solutions $\phi_0(t)$ to Eq. (30) using Eq. (37), with $\eta = 0$ and $\varepsilon = 0$. The functional density $u_0[\phi_0]$ is

$$u_0[\phi_0] = \tfrac{1}{2}K_L\phi_0^2 - 2\gamma_c \cos\{\kappa(\phi_0 + Vt)\} + h\phi_0, \tag{39}$$

where $K_L > 0$ is minus the integral of $T(\mathbf{r})$. The Euler-Lagrange equation corresponding to the potential (39) is

$$K_L\phi_0 = -2\gamma_c\kappa \sin\{\kappa(\phi_0 + Vt)\} - h. \tag{40}$$

Clearly if κ and γ_c are small, $u_0[\phi_0]$ is concave up, and has only a single (global) minimum. On the other hand, if γ_c or κ are sufficiently large, $u_0[\phi_0]$ may have more than one minimum, with all but the lowest energy state being metastable. More than one minimum are possible when

$$\frac{\partial^2 u_0}{\partial \phi_0^2} = K_L + 2\gamma_c\kappa^2 \cos\{\kappa(\phi_0 + Vt)\} \tag{41}$$

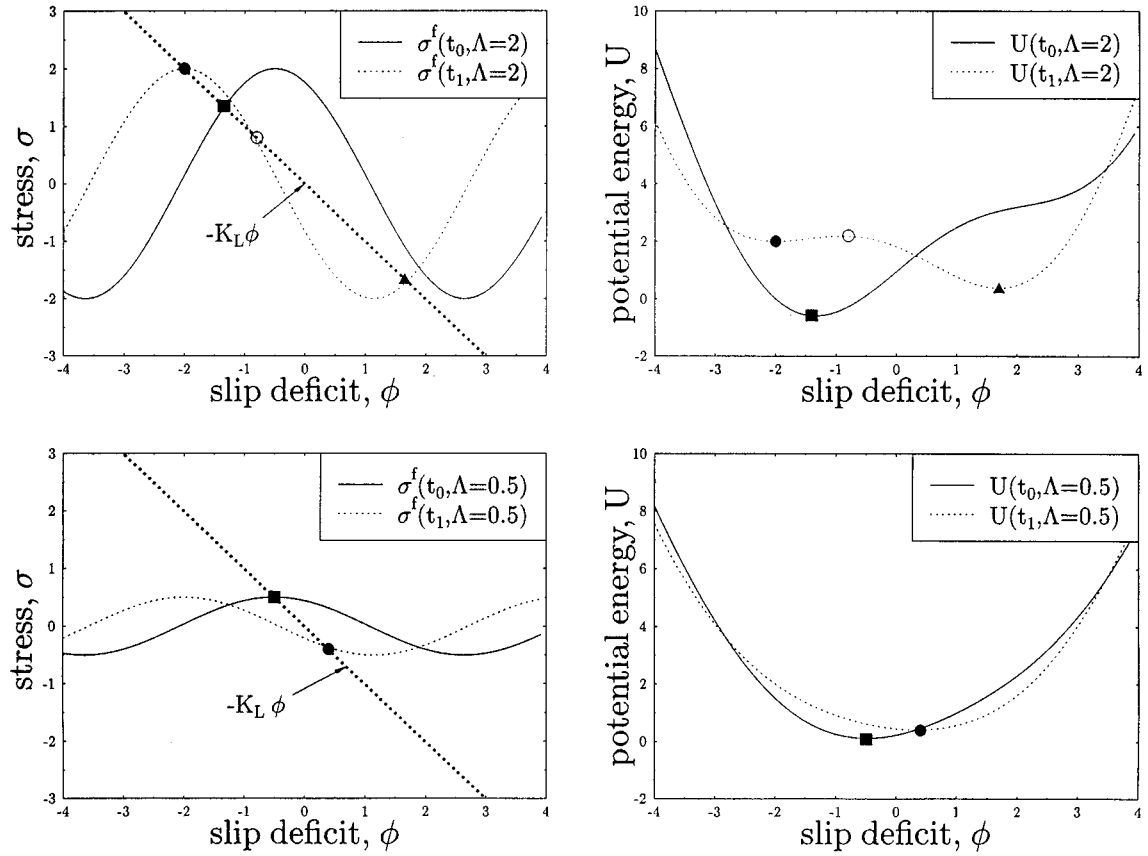

FIG. 4. Stress $\sigma(t)$ and potential energy $U(t)$ against ϕ in mean-field limit, for $\Lambda=2$ (top) and $\Lambda=0.5$ (bottom), and for two distinct times $t_1>t_0$. Top: At time t_0, only one globally stable state exists (square); at time t_1, metastable (filled circle), unstable (open circle), and globally stable (triangle) states now exist. Bottom: At both times t_0 and t_1, only one globally stable state exists (square at t_0 and circle at t_1).

has at least one zero. Metastability can only occur if the parameter $\Lambda>\Lambda_c=1$, where

$$\Lambda=2\gamma_c\kappa^2/K_L\,. \tag{42}$$

As will be clear from the discussion below, $(\Lambda-\Lambda_c)$ can be regarded as a scaling field for this potential. Qualitatively, Λ can be interpreted as indicating the number of local minima. An immediate prediction of the theory is that as the stiffness of the surrounding elastic medium K_L is increased, a transition should occur, from the appearance of sudden unstable jumps (decay from metastability), to stable sliding as Λ decreases. Such a transition is commonly observed [18,20,37,38,47] in laboratory experiments.

The TDW model represented by Eqs. (39) and (40) has the simple geometrical interpretation shown in Fig. 4. The intersection point ϕ^* between the fixed curve and the leftward traveling wave is time dependent. ϕ^* slowly becomes more negative (strain accumulation) until a point is reached at which ϕ^* increases more rapidly in a positive direction (slip event). If the cohesion varies sufficiently in space or in amplitude, leading to $\Lambda>1$, unstable slip can occur at fixed far field displacement in response to the influence of fluctuations (Fig. 4 top). One of these events corresponds to decay from the metastable well. Otherwise, if $\Lambda<1$, the surface slips in a stable manner only in response to increasing far field displacement Vt, regardless of the presence of fluctuations (Fig. 4 bottom). In that case, no metastability is possible.

In addition to $(\Lambda-\Lambda_c)$, time ''t'' can also be regarded as a scaling field for the line of critical points defining the spinodal. It can be observed from Fig. 4 that when the system is in a metastable energy state higher than the global minimum, the passage of time drives down the height of the energy barrier toward the spinodal, and the system nucleates into the lower energy state. This process recurs with period $P=2\pi/(\kappa V)$ so that the spinodal occurs at times $t=t_{\rm SP}+nP, n=$ integer.

VI. EXPANSION ABOUT THE SPINODAL

The equation that describes the nucleation process is identical to that obtained in studies of spinodal nucleation [48], but where the scaling field is proportional to $\delta t=(t_{\rm SP}-t)\,{\rm mod}(P)$. This equation is

$$-K_C\nabla^2\psi+K_LV\delta t-\alpha\psi^2=0. \tag{43}$$

In Eq. (43), $\psi(\mathbf{x},t)$ is the fluctuation of $\phi(\mathbf{x},t)$ about the spinodal value, and K_C and α are nonzero, positive constants.

To derive this result, we begin by considering a model in which long spatial wavelength fluctuations are present. In

that case, the field $\phi=\phi(\mathbf{x},t)$ depends on position, and the Lyapunov functional density u_0 is modified by the presence of a term $K_C|\nabla\phi|^2$

$$U'[\phi]=\int\int\{\tfrac{1}{2}[K_L\phi^2+K_C|\nabla\phi|^2] - 2\gamma_c\cos[\kappa\{\phi+Vt\}]+h\phi\}. \quad (44)$$

The corresponding Euler-Lagrange equation is

$$K_L\phi-K_C\nabla^2\phi+2\gamma_c\kappa\sin\{\kappa(\phi+Vt)\}+h=0. \quad (45)$$

In Eqs. (44) and (45), the constant K_C is proportional to the second moment of the stress Green's function $T(\mathbf{r})$. Denoting the spatially constant value of ϕ_0 at the spinodal $t_{\rm SP}$ by $\Phi(t_{\rm SP})$, we expand about the spinodal by writing

$$\phi(\mathbf{x},t)=\Phi(t_{\rm SP})+\psi(\mathbf{x},t), \qquad t=t_{\rm SP}-\delta t, \quad (46)$$

where $|\psi(\mathbf{x},t)|\ll|\Phi|$, and $\kappa V\delta t\ll 2\pi$. Note that the spatial average $\langle\psi(\mathbf{x},t_{\rm SP})\rangle$ of $\psi(\mathbf{x},t_{\rm SP})$ must vanish at the spinodal, which from Eq. (43) implies that $\psi(\mathbf{x},t_{\rm SP})$ must vanish identically. Therefore, we expect that

$$\psi(\mathbf{x},t)\propto\delta t^r, \quad (47)$$

where the exponent $r>0$.

The first step in obtaining Eq. (43) is to solve the pair of equations defining the spinodal to obtain the values of Φ and $t_{\rm SP}$

$$K_L\Phi+2\gamma_c\kappa\sin\{\kappa(\Phi+Vt_{\rm SP})\}+h=0, \quad (48)$$

$$K_L+2\gamma_c\kappa^2\cos\{\kappa(\Phi+Vt_{\rm SP})\}=0. \quad (49)$$

The second step is to substitute the expressions (46) into Eq. (45)

$$K_L\{\Phi+\psi\}-K_C\nabla^2\psi+2\gamma_c\kappa\sin\{\kappa(\Phi+\psi+Vt_{\rm SP}-V\delta t)\} +h=0. \quad (50)$$

The third term can be written as

$$\sin\{\kappa(\Phi+\psi+Vt_{\rm SP}+V\delta t)\} = \sin\{\kappa(\Phi+Vt_{\rm SP})\}\cos\{\kappa(\psi-V\delta t)\} + \cos\{\kappa(\Phi+Vt_{\rm SP})\}\sin\{\kappa(\psi-V\delta t)\}. \quad (51)$$

Using the fact that ψ and δt are small, we approximate the right hand side of Eq. (51) as

$$\sin\{\kappa(\Phi+Vt_{\rm SP})\}[1-(\kappa^2/2)\{\psi-V\delta t\}^2] + \cos\{\kappa(\Phi+Vt_{\rm SP})\}\{\kappa(\psi-V\delta t)\}. \quad (52)$$

Substitution of Eq. (52) into Eq. (49) and expanding yields the equation

$$[K_L\Phi+2\gamma_c\kappa\sin\{\kappa(\Phi+Vt_{\rm SP})\}+h]-K_C\nabla^2\psi - \psi[K_L+2\gamma_c\kappa^2\cos\{\kappa(\Phi+Vt_{\rm SP})\}] - 2\gamma_c\kappa^2V\delta t\{\cos[\kappa(\Phi+Vt_{\rm SP})]\} - \gamma_c\kappa^3\{\psi^2-\psi V\delta t+(V\delta t)^2\}\sin\{\kappa(\Phi+Vt_{\rm SP})\}=0. \quad (53)$$

The first and third terms, in the square brackets of Eq. (53), are identically zero, by virtue of Eqs. (48) and (49). Using Eq. (49) to rewrite the term proportional to δt, the remaining nonzero parts of Eq. (53) are

$$-K_C\nabla^2\psi+K_LV\delta t-\gamma_c\kappa^3\{\psi^2-\psi V\delta t+(V\delta t)^2\} \times\sin\{\kappa(\Phi+Vt_{\rm SP})\}=0. \quad (54)$$

Near the spinodal we search for scaling solutions of Eq. (54), which in addition to Eq. (47) implies that spatial coordinates $\mathbf{x}$ vary significantly on a spatial (correlation) length scale ξ

$$\xi\propto\delta t^s. \quad (55)$$

If Eqs. (47) and (55) are inserted into Eq. (54), it can be seen that Eq. (43) is obtained self-consistently, with $r=1/2$ and $s=-1/4$, and with all other terms being of higher order in δt and therefore negligible as $t\to t_{\rm SP}$. Thus the solution $\psi(\mathbf{x},t)\sim(K_LV\delta t)^{1/2}\tilde{\psi}(|\mathbf{x}|/\xi)$, where the correlation length $\xi\sim(K_LV\delta t)^{-1/4}$ and $\tilde{\psi}$ is nonzero and bounded at $t=t_{\rm SP}$. This is precisely the kind of low-amplitude, large spatial-extent solution that has been observed in recent field data [10]. The constant α in Eq. (43) is $\alpha=\gamma_c\kappa^3\sin\{\kappa(\Phi+Vt_{\rm SP})\}$, which is positive and does not vanish at the spinodal. The latter can be seen by making use of Eqs. (48) and (49).

VII. IMPLICATIONS OF TDW MODELS FOR SCALING

Because Eq. (43) has been extensively studied in the literature in other problems [35,48], a number of results are immediately available, and predictions can be made. For example, the frequency of spinodal fluctuations $n(A)$ of area A, which are realized here as clusters of failed sites, is given by the Fisher-Stauffer relation [49]

$$n(A,\delta t)=\frac{n_0}{A\zeta}\exp\{-k[K_LV\delta t]^{1/\sigma_s}A\}. \quad (56)$$

The parameter k is a constant determined by fitting the data. The exponent σ_s is the surface exponent, and the exponent ζ is either $\zeta=\tau-1$ or $\zeta=\tau$, in terms of the Fisher-Stauffer exponent [49] τ. The relation $\zeta=\tau$ characterizes fluctuations (earthquakes) about the spinodal, whereas the relation $\zeta=\tau-1$ describes the frequency of ''arrested'' nucleation events (mainshocks) [22,23].

Formally, one can also expand about the spinodal for time intervals following $t_{\rm SP}$. Then instead of Eq. (46), time is expressed as

$$t=\delta t-t_{\mathrm{SP}}. \tag{57}$$

The entire development of the preceding section follows through as above, with δt replaced by $-\delta t$ in the spinodal equation (38) and in the Fisher-Stauffer relation (56).

However, the validity of expanding about the spinodal for $t>t_{\mathrm{SP}}$ can be questioned on physical grounds. In particular, the applicability of the Fisher-Stauffer relation (56) is not clear, since it was originally proposed to describe fluctuations in systems residing at local minima (equilibrium and metastable equilibrium). For $t>t_{\mathrm{SP}}$, the metastable minimum no longer exists. However, it will be shown (see discussion below) that the Fisher-Stauffer relation can be used to obtain an Omori-type aftershock decay relation for foreshocks. It is therefore tempting to propose the hypothesis that Eq. (56) also describes the fluctuations for times immediately after the spinodal as well, based on the fact that Eq. (57) leads to the same kind of equation as Eq. (43), but with δt redefined. Note that evidence for the existence of Fisher-Stauffer scaling in the unstable region has been found independently in simulations of systems undergoing spinodal decomposition [50,51] for short time intervals following the quench.

We can obtain values for all the scaling exponents, and from these predict a range for the Gutenberg-Richter b value, by making use of standard scaling relations known for systems with two scaling fields. We define two additional exponents γ and β for the order parameter $\psi(\mathbf{x},t)$ and the susceptibility $\chi(\mathbf{x},t)$ of $\psi(\mathbf{x},t)$ to small changes in the scaling field $[K_L V\delta t]$

$$\psi(\mathbf{x},t)\sim(K_L V\delta t)^{1/2}\tilde{\psi}(|\mathbf{x}|/\xi)\propto[K_L V\delta t]^{\beta}, \tag{58}$$

$$\chi(\mathbf{x},t)\sim\frac{\partial\psi(\mathbf{x},t)}{\partial[K_L V\delta t]}\propto[K_L V\delta t]^{-\gamma}. \tag{59}$$

From these definitions, $\beta=1/2$, and $\gamma=1/2$, and using the scaling relations [49]

$$\frac{\tau-2}{\sigma_s}=\beta, \tag{60}$$

$$\frac{3-\tau}{\sigma_s}=\gamma, \tag{61}$$

we find $\tau=5/2$, $\sigma_s=1$, i.e., the ''magnetic'' values of τ, σ_s. We now consider two problems, (1) Omori's law and (2) the Gutenberg-Richter b value.

Omori's law. The rate at which the number of aftershocks decay following a major earthquake obeys a relationship first observed by Omori following the 1891 Nobi, Japan, earthquake

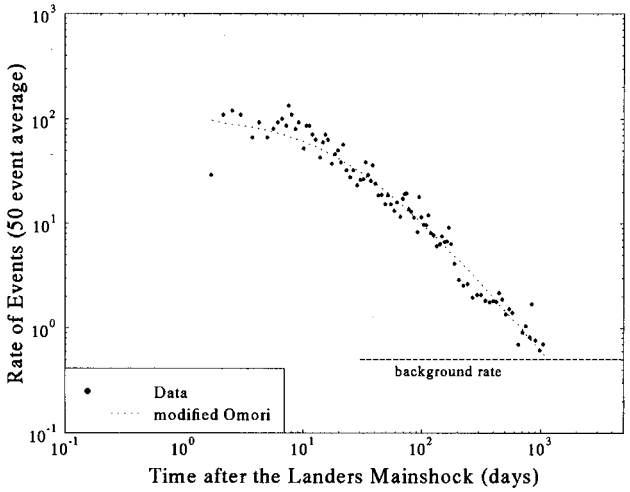

FIG. 5. Frequency of aftershocks as a function of time for the June 28, 1992 Landers earthquake.

$$n_{as}=\frac{K}{(c+\Delta t_{ms})^{p}}. \tag{62}$$

Here n_{as} is the rate of aftershock occurrence, c and K are constants, $\Delta t_{\mathrm{eq}}=t-t_{\mathrm{ms}}$ is the time interval since the mainshock, and p is an exponent usually found from observations [9,52,53] to be $p\approx 1$. Equation (62) is essentially an inverse time law modified to account for the fact that the rate of aftershock occurrence remains finite at times just after the mainshock. The validity of Eq. (62) is illustrated in Fig. 5, which is a log-log plot of frequency of all aftershocks against time following the June 28, 1992 Landers earthquake. The temporal decay of activity fits a line with a slope of $p\approx 1$ as illustrated.

Recently it has been realized that the increase in the rate of foreshocks n_{fs} prior to the mainshock follows the same form [54,55] of law as Eq. (61), with Δt_{eq} replaced by $-\Delta t_{\mathrm{eq}}$, and with an exponent p'. Moreover, it is also observed that $p'=p\approx 1$, although the constants K and c depend on the individual foreshock or aftershock sequence.

Using our results, we can obtain a prediction for the form of an Omori's rate law, while remembering the caveats from discussion just below Eq. (57). We first identify the observationally defined interval $\Delta t_{\mathrm{eq}}=t-t_{\mathrm{ms}}$ since the mainshock with the time interval since the spinodal (at which scaling is observed), thus $\Delta t_{\mathrm{eq}}\approx-\delta t$. Consider first the problem of foreshocks, in which Δt_{eq} is replaced by $-\Delta t_{\mathrm{eq}}$. To calculate the frequency of events at time δt in terms of the frequency at time $\delta t=0$, we use the event frequency relation (56) to integrate over a band of events lying between area $(A_{\min},A_{\max})$

$$\int_{A_{\min}}^{A_{\max}}\frac{n(A,\delta t)}{n(A,0)}dA=\left\{\frac{\exp[-k(K_L V\delta t)^{1/\sigma_s}A_{\min}]-\exp[-k[K_L V\delta t]^{1/\sigma_s}A_{\max}]}{k[K_L V\delta t]^{1/\sigma_s}}\right\}. \tag{63}$$

We see that for times $\delta t > 0$, the frequency varies with time according to $(\delta t)^{-1/\sigma_s}$, modified by an exponential decay. Since $\sigma_s = 1$, an Omori p' value of $p' = 1/\sigma_s = 1$ is predicted, in agreement with observation [9,52]. Calculation of the aftershock rate is carried out in the same way, with δt replaced by $-\delta t$. The value of p is the same, and $p = p' = 1/\sigma_s = 1$ is predicted, in agreement with observations of real fault systems.

Integrating over all events up to the size of the mainshock, one finds a foreshock (aftershock) frequency

$$n_{\rm tot}(\delta t) = n_{\rm tot}(0)\left\{\frac{1-\exp[-k(K_L V \delta t)^{1/\sigma_s} A_{\rm max}]}{k[K_L V \delta t]^{1/\sigma_s}}\right\}. \quad (64)$$

This relationship behaves asymptotically as $1/\delta t^{1/\sigma_s}$ for ''large'' δt, where the approach to the asymptotic form is controlled by the size of $A_{\rm max}$, the mainshock area. Again $p' = p = 1/\sigma_s = 1$ is found. Recall that Eq. (64), which was obtained from Eq. (56), is valid only for time intervals so small that $\kappa V \delta t \ll 2\pi$. Since $2\pi/\kappa$ is the nominal slip distance in the earthquake, $2\pi/(\kappa V) = T_{\rm rec}$, where $T_{\rm rec}$ is the nominal recurrence time for the largest earthquakes. Thus the condition for small δt reduces to $\delta t \ll T_{\rm rec}$. Observations of real earthquakes [9,56,57] indicate that frequency of seismic activity (aftershocks) has the characteristic $\sim 1/\delta t^p$ scaling form only when this condition is satisfied. Finally, typical values of $A_{\rm max}$ are extremely large, of the order of 10^8 m^2 for a magnitude 6 earthquake. Thus the approach to the asymptotic form $1/\delta t^{1/\sigma_s}$ is expected to be fast compared to the total time $\delta t^{\rm max}$ over which Eq. (64) is valid, as observed [9].

On the basis of empirical observations, a stretched exponential form for foreshock buildup and aftershock decay very similar to Eq. (63) has been suggested [56,57] that fits seismicity data as well or better than the classical Omori law. The corresponding cumulative frequency of events on the interval $(0, -\delta t)$, which we denote by $N_{\rm tot}$ is easily found for the expected value $1/\sigma_s = 1$

$$N_{\rm tot}(\delta t) = \lim_{\varepsilon \to 0}\left(\frac{n_{\rm tot}(0)}{k K_L V}\right)\{\ln(-\delta t/\varepsilon) - \Gamma_{\rm inc}(\varepsilon, -\delta t)\}. \quad (65)$$

Here $\Gamma_{\rm inc}$ is the incomplete γ function [58]. It can easily be seen that $N_{\rm tot}(\delta t)$ has the well defined limit $N_{\rm tot}(0) = 0$.

Equations (63)–(65) for aftershocks and their counterparts for foreshocks also predict that the rate of large aftershocks decays more rapidly than smaller events as $-\delta t$ increases. Similarly, the rates of large foreshocks increase more rapidly than do the rates of small events as δt decreases. To test this prediction, we plotted the cumulative distribution for Landers aftershocks with time, for groups of equal numbers of events (Fig. 6). It can be seen from the data that the larger aftershocks do relax much more rapidly with time than the smaller events, although the effect is overpredicted by Eq. (63). We point out that modifications of inverse power laws in δt have been shown to be useful in earthquake forecasting [59,60]. These authors show that in some cases, leading order corrections to the p value take the form of complex exponents. We will address these ideas in a future publication [61].

Gutenberg-Richter b value. The Gutenberg-Richter relation $N_{\rm GR}(m)$ is technically the function that describes the tail of a cumulative distribution. Using parameters $\{b, a\}$, $N_{\rm GR}(m)$ is the cumulative frequency of events with magnitude larger than some value m

$$\ln N_{\rm GR}(m) = -bm + a. \quad (66)$$

Observations indicate that $b \sim 1$, but this simple statement obscures the fact that observed values of b can vary from roughly 0.6 up to 2 (see discussion below). The b value can be related to, but is not the same as, the parameter in the relation between frequency and radiated energy E_R (see, for example, Ref. [52] for details). The latter has sometimes been quoted in the nonseismological literature as the ''b value,'' when in fact it is not. A careful distinction should be made between the total energy lost $E_{\rm tot}$ (as in a sandpile avalanche), and the radiated energy E_R.

We can use the Fisher-Stauffer relation (56) to obtain a scaling relationship for b in terms of ζ and another exponent c, which defines the scale dependence of the seismic moment M_0 on the event area A

$$M_0 \propto A^c. \quad (67)$$

Together with the moment-magnitude relation [62]:

$$m = \frac{2}{3}\ln M_0 - 10.7, \quad (68)$$

we find by integrating Eq. (56) over areas $[A, \infty)$, using Eqs. (67) and (68), and equating powers of the area that

$$b = \frac{3(\zeta - 1)}{2c}. \quad (69)$$

Recent works [63–69] suggests that c lies between 1 and 3/2. ζ can range from 3/2–5/2, depending on whether mainshocks (arrested nucleation events [22,23]) or foreshocks and aftershocks (spinodal fluctuations [22,23]) are of interest. Thus b is predicted to range from (0.5, 2.25). Observed values [65,66,68] are typically in the range from 0.8–2.1, although declustered values [55] can be as low as 0.6, whereas swarms of events can sometimes have b values [9] up to perhaps as large as 2. The predictions of our theory thus bracket the range of the observed values.

Simulations

We carried out a series of simulations to check our results, and we give an example that lends support to the results we found from analyzing Eq. (69). We solved the evolution equation (38) using a modified Newton's method [61] including noise terms, on a 100×100 lattice of sites using an interaction given by K_C/r^3, with each block connected to 13^2 sites. The quantities γ_c and κ were held fixed, producing a simple time dependent potential. Note that the cohesive forces are not scale independent as perhaps is implied by the observations of fractal topography on fault surfaces [25]. Sources of noise in the simulation were provided both from random phases ε that changed after each site decayed from the local minimum, as well as noise η inherent in the modi-

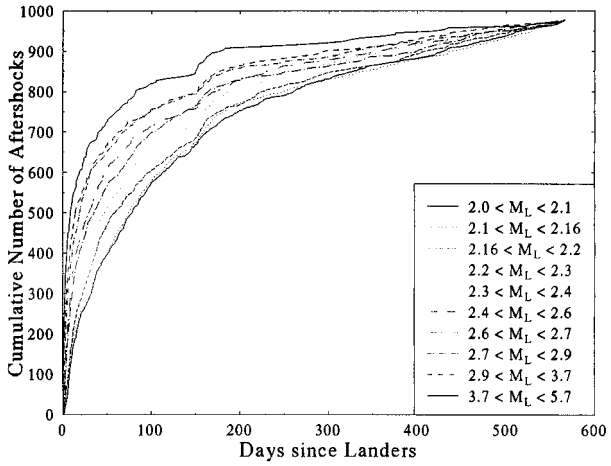

FIG. 6. Cumulative Landers aftershocks in days since mainshock. All magnitude bins have ~970 events. The largest event bins clearly relax the most rapidly, as predicted by Eq. (27).

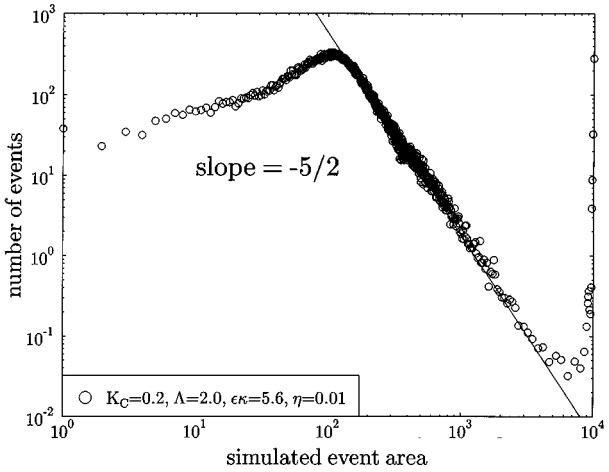

FIG. 7. Number of simulated events against area of simulated event on a log-log plot.

fied Newton method used for solving the equations. Figure 7 shows a plot of frequency of occurrence against event size. There are three regions apparent on the plot. The region to the left of the local maximum near $A=100$, which is determined by the noise amplitude $\eta=0.01$, is noise dominated. The region between $A=100$ and $A\sim5000$ is the scaling region that represents spinodal fluctuations, and has a slope $\zeta=\tau=2.5$ as predicted. The region $A>4000$ represents nucleation events, in which large sections of the lattice decay from the metastable well simultaneously.

Figure 8 is a cumulative Gutenberg-Richter plot for the same simulations as in Fig. 7, showing the plot with and without nucleation events included. The slope of the scaling region representing spinodal fluctuations is $b\sim2.2$. This value can be checked against Eq. (69) using $\zeta=\tau=2.5$ and $c\sim1$, giving a predicted value for $b=2.25$. The value $c\sim1$ arises for our simple model (38) because γ_c is neither site dependent nor self-similar. It should be pointed out that these values for b (and p) were obtained for a model of only a single isolated fault. The finite extent of real fault segments, and the relative numbers of small faults to larger ones will clearly affect the scaling distributions to some degree. We plan to address this fundamental problem in future work.

VIII. FOKKER-PLANCK EQUATION AND NUCLEATION

Under the conditions described in Eqs. (35)–(37), it is straightforward to show that there exists an associated Fokker-Planck equation describing the time variation of the probability density $f[\phi]$ on the slip deficit variables [70]. The stationary solution of this equation is

$$f[\phi]=Z^{-1}\exp\{-\beta U[\phi]\}, \tag{70}$$

$U[\phi]$ thus plays the role of an equilibrium ''free energy functional,'' the normalization constant Z plays the role of the partition function of equilibrium statistical mechanics, and the noise correlation amplitude β plays the role of an inverse temperature.

As a result, for given $\Lambda>1$, the lifetime in the metastable state Γ_m can be obtained by reading off the results from Refs. [48,71]

$$\Gamma_m\sim\exp\{K_C(K_LV\delta t)^{3/2-d/4}\}, \tag{71}$$

where d is the dimension of space ($d=2$ for a planar fault). Moreover, one expects [48,71] that nucleation will occur near the Becker-Döring limit

$$K_C(K_LV\delta t)^{3/2-d/4}\propto\beta^{-1}, \tag{72}$$

where the constant of proportionality is in the range of 2–4.

Referring back to the discussion associated with Eqs. (1)–(6), it is now clear that the existence of Boltzmann-type distributions is associated with the presence of long range interactions and the mean-field regime. Note that $1/r^3$ interactions with physical cutoffs at both small and large wavelengths are the physics by which defects in elastic solids interact. We therefore expect that the results of these mean-field theories will be applicable to earthquake fault systems. More importantly, it can now be seen that the TDW model leads to methods of analysis for earthquake faults that are often isomorphic to those used in equilibrium statistical mechanics. In particular, we should fully expect to see nucleation phenomena (characteristic earthquakes) similar to that seen in equilibrium systems.

IX. SUMMARY AND REMARKS ON STATE-VARIABLE FRICTION AND NEURAL MODELS

We have discussed a number of models for friction, and have shown that the statistical mechanics of these models is amenable to analysis using standard techniques. We have also shown that CA models can be treated as equilibrium models in the mean-field regime, which constitute the space of the models of interest for real elastic systems. These mean-field models can be described by a spatially and temporally coarse grained energy functional that leads to an Itô-Langevin equation. We also described a model recently introduced elsewhere [11], the TDW model, and showed that a Lyapunov potential energy functional could be defined that plays the role of an equilibrium free energy functional. Associated probability distributions, scaling exponents, and predictions that compare favorably with data were also intro-

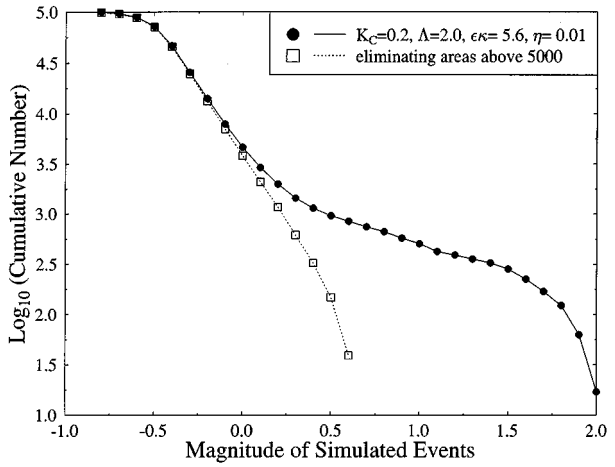

FIG. 8. Gutenberg-Richter plot of cumulative number of simulated events plotted against event magnitude. Filled circles include events $A>5000$, open squares do not.

duced, derived, and discussed.

One of the questions that has been raised by a variety of authors [17–19,27] is whether simple stick-slip friction, as used in the CA models discussed in this paper, is a valid physical mechanism for describing frictional sliding. Many of these authors in fact advocate a slip weakening friction law, such as the TDW model, or a velocity weakening law, such as those discussed in Refs. [2,18] and [19] (see, for example, Eqs. (75) and (76) below). However, recent work by Schmittbuhl, Vilotte, and Roux [72] indicates that a large class of velocity weakening friction laws iterate to the classical stick-slip friction law under a renormalization group rescaling transformation. This result clearly indicates that if a model is sufficiently coarse grained spatially, the stick-slip law should be physically justified.

Two final remarks are in order. In the following, a comparison is provided between our model and another commonly used friction model, as well as some comments on the possible applicability of traveling density wave models to integrate-and-fire neural models.

State-variable friction. As mentioned briefly in the Introduction, another model that is frequently used to understand sliding friction is the phenomenological rate and state-variable law. This friction law has been developed by the use of laboratory experiments generally limited to clean, dust free, smooth rock samples. In this lumped-parameter model, the spatially averaged friction force σ^f on a sliding laboratory block is represented by the equations

$$\sigma^f=\sigma_0^f+A\ \ln(V/V_0)+\theta, \tag{73}$$

$$\frac{d\theta}{dt}=\frac{-V}{d_c}[\theta+B\ \ln(V/V_c)], \tag{74}$$

where σ_0^f, A, B, V_0, and d_c are constants to be determined from data. The quantity $\theta(t)$ is a ''state variable,'' whose physical meaning has been variously postulated to be ''asperity contact time'' [17], the amplitude [25] of the fundamental Fourier component of the slip deficit ϕ, the separation between the sliding surfaces [46], as well as other meanings (see the bibliography in Ref. [14]). In order for instabilities to occur, $A-B>0$. It should be noted that in the experiments leading to Eqs. (73) and (74), the stiffness of the laboratory apparatus is arranged in such a way that it is very large compared to the stiffness of the sliding sample. In that case, and by virtue of the quasistatic nature of the sliding experiments, it is usually assumed that (1) $V=ds/dt$, where s is the average slip of the sliding surface, (2) that a steady state regime is eventually achieved, and (3) that $\sigma^f=\sigma^e$.

By a suitable redefinition of state variable, Eq. (73) can be put into the suggestive form

$$\sigma^f=\sigma_0^f+A\,\theta'=\sigma^e, \tag{75}$$

whereas Eq. (74) can be reduced to

$$\frac{d\theta'}{dt}=\left(\frac{-V}{d_c}\right)[\theta'+\ln(V/V_c)^{1-B/A}], \tag{76}$$

where

$$\theta'=\ln[(V/V_c)\,\phi^{1/A}]. \tag{77}$$

Now we show that the TDW model can be put into a form similar to Eqs. (76) and (77). Expanding Eq. (25) about the mean-field regime, in the presence of appropriate cutoffs, yields the expression

$$\sigma^e=\sigma_B-K_L\phi_0(t). \tag{78}$$

Similarly, using the linearized evolution equation for $\phi(t)$ corresponding to Eq. (38), we obtain the equation

$$\frac{d\phi_0}{dt}=-(K_L+2\,\gamma_c\kappa^2)[\phi_0+Vt]-h. \tag{79}$$

If γ_c and h are assumed to depend on the sliding velocity V, there is a similarity between Eqs. (75) and (78), and between Eqs. (79) and (76), if $\phi_0(t)$ is identified with the state variable $\theta'(t)$. There is one major difference, however, in that Eq. (79) predicts a nontrivial dependence on the far field displacement $d_{\rm far}=Vt$, whereas Eq. (76) does not. It is interesting that recent laboratory experiments [20,21] actually indicate a dependence of friction on $d_{\rm far}$ as a result of the inevitable processes of wear that irreversibly deform and alter the sliding surfaces as slip progresses.

Neural models. An important property of integrate-and-fire neural models is that they possess a periodic limit cycle attractor [5,73,74]. It should be noted that periodic behavior is sometimes approximately observed in real earthquakes as well, such as at Parkfield, California [9]. Under the Itô-Langevin dynamics (32), the Lyapunov functional $U[\phi(t)]$ will undergo a ''downhill march'' on its energy landscape in the zero noise limit. This property of $U[\phi(t)]$ is obvious in light of the definition of the dynamics (34) and (35). Moreover, because U is bounded from below, it can be shown [5,73] that $U[\phi(t+P)]\leqslant U[\phi(t)]$, and the system approaches a periodic limit cycle. This will also be true for systems with quenched disorder. Systems with these properties can be used to model integrate-and-fire neurons

[5,73,74]. If ϕ is identified with cellular potential, and V with injected current divided by cell capacitance [73] for an integrate-and-fire neuron Eq. (8) can be regarded as an explicitly, rather than the usual implicit [5] equation for the evolution of the cellular potential. Decay of a neuron from metastability is then identified with the transmission of an action potential. We suggest that the network learning problem might be made easier for models of this type by the use of the explicit evolution equation.

ACKNOWLEDGMENTS

Work carried out by J.B.R. and S.G. was supported under U.S. Department of Energy Grant No. DE-FG03-95ER14499 to the Cooperative Institute for Research in Environmental Sciences at the University of Colorado, and NSF Grant No. EAR-9526814. The work of W.K. and C.D.F. was supported under U.S. Department of Energy Grant No. DE-FG02-95ER14498 to the Physics Department and Center for Computational Science at Boston University.

[1] P. Bak, C. Tang, and K. Weisenfield, Phys. Rev. Lett. **59**, 381 (1987).
[2] R. Burridge and L. Knopoff, Bull. Seismol. Soc. Am. **57**, 341 (1967).
[3] C. Tang and P. Bak, J. Stat. Phys. **51**, 797 (1988).
[4] J. B. Rundle and D. D. Jackson, Bull. Seismol. Soc. Am. **67**, 1363 (1977).
[5] A. V. M. Herz and J. J. Hopfield, Phys. Rev. Lett. **75**, 1222 (1995).
[6] J. S. Urbach, R. C. Madison, and J. T. Markert, Phys. Rev. Lett. **75**, 276 (1995).
[7] A. D. Gopal and D. J. Durian, Phys. Rev. Lett. **75**, 2610 (1995).
[8] H. M. Jaeger, S. R. Nagel, and R. P. Behringer, Phys. Today **49** (4), 32 (1996).
[9] C. H. Scholz, *The Mechanics of Earthquakes and Faulting* (Cambridge University, Cambridge, England, 1990).
[10] W. Ellsworth and G. Beroza, Science **268**, 861 (1995).
[11] J. B. Rundle, W. Klein, and S. Gross, Phys. Rev. Lett. **76**, 4285 (1996).
[12] G. Gruner, *Density Waves in Solids* (Addison-Wesley, Reading, MA, 1994).
[13] D. S. Fisher, Phys. Rev. B **31**, 1396 (1985).
[14] J. B. Rundle and W. Klein, Rev. Geophys. Space Phys., Suppl., July, 283 (1995).
[15] J. B. Rundle, W. Klein, S. Gross, and D. L. Turcotte, Phys. Rev. Lett. **75**, 1658 (1995).
[16] J. M. Carlson and J. S. Langer, Phys. Rev. Lett. **62**, 2632 (1989).
[17] J. H. Dieterich, J. Geophys. Res. **84**, 2161 (1979).
[18] A. Ruina, J. Geophys. Res. **88**, 10359 (1983).
[19] J. R. Rice, J. Geophys. Res. **98**, 9885 (1993).
[20] N. M. Beeler, T. E. Tullis, and J. D. Weeks, Geophys. Res. Lett. **21**, 1987 (1994).
[21] N. M. Beeler, T. E. Tullis, M. L. Blanpied, and J. D. Weeks, J. Geophys. Res. **101**, 8697 (1996).
[22] W. Klein, J. B. Rundle, and C. D. Ferguson, Phys. Rev. Lett. **78**, 3793 (1997).
[23] C. D. Ferguson, W. Klein, and J. B. Rundle (to be published).
[24] J. B. Rundle and W. Klein, Phys. Rev. Lett. **63**, 171 (1989).
[25] J. B. Rundle and S. R. Brown, J. Stat. Phys. **65**, 403 (1991).
[26] J. B. Rundle and W. Klein, J. Stat. Phys. **72**, 405 (1993).
[27] Y. Ben-Zion and J. R. Rice, J. Geophys. Res. **98**, 14109 (1993).
[28] G. Narkounskaia, J Huang, and D. L. Turcotte, J. Stat. Phys. **67**, 1151 (1992).
[29] H. Nakanishi, Phys. Rev. A **43**, 6613 (1990).
[30] A. Gabrielov, W. Newman, and L. Knopoff, Phys. Rev. E **50**, 188 (1994).
[31] G. Morein, D. L. Turcotte, and A. Gabrielov (unpublished).
[32] K. Huang, *Statistical Mechanics* (Wiley, New York, 1987).
[33] J. B. Rundle and D. L. Turcotte, in *Contributions of Space Geodesy to Geodynamics: Crustal Dynamics*, edited by D. E. Smith and D. L. Turcotte, Geodynamics Ser. Vol. 23 (American Geophysical Union, Washington, DC, 1993).
[34] S. Ross, *A First Course in Probability* (MacMillan, New York, 1994).
[35] T. Ray and W. Klein, J. Stat. Phys. **53**, 773 (1988).
[36] D. P. Hill *et al.*, Science **260**, 1617 (1993).
[37] F. P. Bowden and D. Tabor, *The Friction and Lubrication of Solids* (Clarendon, Oxford, 1950).
[38] E. Rabinowicz, *Friction and Wear of Materials* (Wiley, New York, 1965).
[39] J. N. Brune, S. Brown, and P. A. Johnson, Tectonophysics **218**, 59 (1993).
[40] V. C. Li, in *Fracture Mechanics of Rock*, edited by B. K. Atkinson (Academic, London, 1987), pp. 351–428.
[41] T. F. Wong, in *Earthquake Source Mechanics*, edited by S. Das, J. Boatwright, and C. H. Scholz (American Geophysical Union, Washington, DC, 1986), pp. 1–12.
[42] J. D. Byerlee, Tectonophysics **9**, 475 (1970).
[43] J. B. Rundle, J. Geophys. Res. **93**, 6237 (1988).
[44] J. B. Rundle, J. Geophys. Res. **94**, 2839 (1989).
[45] G. P. Tolstov, *Fourier Series* (Dover, New York, 1962).
[46] J. Lomnitz-Adler, J. Geophys. Res. **96**, 6121 (1991).
[47] T. Baumberger, F. Heslot, and B. Perrin, Nature (London) **367**, 544 (1994).
[48] W. Klein and C. Unger, Phys. Rev. B **28**, 445 (1983).
[49] D. Stauffer and A. Aharony, *Introduction to Percolation Theory* (Taylor and Francis, London, 1991).
[50] J. B. Ross, Ph.D. thesis, Boston University, 1993.
[51] N. Gross, W. Klein, and K. Ludwig, Phys. Rev. Lett. **73**, 2639 (1944).
[52] C. F. Richter, *Elementary Seismology* (Freeman, San Francisco, 1958).
[53] C. Kisslinger, Adv. Geophys. **38**, 1 (1996).
[54] T. Yamashita and L. Knopoff, Geophys. J. R. Astron. Soc. **91**, 13 (1987).
[55] L. M. Jones, R. Console, F. Di Luccio, and M. Murru, Trans. Am. Geophys. Union EOS Suppl. **76**, F388 (1995).
[56] C. Kisslinger, J. Geophys. Res. **98**, 1913 (1993).
[57] S. J. Gross and C. Kisslinger, Bull. Seismol. Soc. Am. **84**, 1571 (1994).
[58] W. H. Press, B. P. Flannery, S. A. Teukolsky, and W. T. Vet-

terling, *Numerical Recipes* (Cambridge University, Cambridge, England, 1986).
[59] C. G. Sammis, D. Sornette, and H. Saleur, in *Reduction and Predictability of Natural Disasters*, edited by J. B. Rundle, D. L. Turcotte, and W. Klein, Santa Fe Institute Series in Sciences of Complexity (Addison-Wesley, Reading, MA, 1996), Vol. XXV.
[60] D. Sornette, A. Johansen, A. Arneodo, J. F. Muzy, and H. Saleur, Phys. Rev. Lett. **76**, 251 (1996).
[61] S. J. Gross and J. B. Rundle (unpublished).
[62] T. C. Hanks and H. Kanamori, J. Geophys. Res. **84**, 2348 (1979).
[63] J. B. Rundle, J. Geophys. Res. **94**, 12337 (1989).
[64] J. B. Rundle, J. Geophys. Res. **98**, 21943 (1993).
[65] J. F. Pacheco, C. H. Scholz, and L. R. Sykes, Nature (London) **355**, I71 (1992).
[66] E. G. Triep and L. R. Sykes (unpublished).
[67] S. J. Gross, in *Reduction and Predictability of Natural Disasters*, edited by J. B. Rundle, D. L. Turcotte, and W. Klein, Santa Fe Institute Series in Sciences of Complexity (Addison-Wesley, Reading, MA, 1996), Vol. XXV.
[68] B. Romanowicz, Geophys. Res. Lett. **19**, 481 (1992).
[69] B. Romanowicz and J. B. Rundle, Bull. Seismol. Soc. Am. **83**, 1294 (1993).
[70] H. Haken, Synergetics (Springer-Verlag, Berlin, 1983).
[71] C. Unger and W. Klein, Phys. Rev. B **29**, 2698 (1984).
[72] J. Schmittbuhl, J.-P. Vilotte, and S. Roux, J. Geophys. Res. **101**, 13911 (1996).
[73] J. B. Rundle and J. J. Hopfield (unpublished).
[74] J. J. Hopfield, Phys. Today **47** (2), 40 (1994).